A&A 545, A2 (2012)
DOI: 10.1051/0004-6361/201219172

Astronomy & Astrophysics

Submillimetric spectroscopic observations of volatiles in comet C/2004 Q2 (Machholz)*

M. de Val-Borro[1,†], P. Hartogh[1], C. Jarchow[1], M. Rengel[1], G. L. Villanueva[2,3], M. Küppers[4], N. Biver[5], D. Bockelée-Morvan[5], and J. Crovisier[5]

[1] Max Planck Institute for Solar System Research, Max-Planck-Str. 2, 37191 Katlenburg-Lindau, Germany
e-mail: [deval;hartogh;jarchow;rengel]@mps.mpg.de
[2] Solar System Exploration Division, NASA Goddard Space Flight Center, Greenbelt, MD 20771, USA
e-mail: geronimo.villanueva@nasa.gov
[3] Department of Physics, Catholic University of America, Washington, DC 20064, USA
[4] Rosetta Science Operations Centre, European Space Astronomy Centre, European Space Agency, PO Box 78, 28691 Villanueva de la Cañada, Madrid, Spain
e-mail: michael.kueppers@sciops.esa.int
[5] LESIA, Observatoire de Paris, CNRS, UPMC, Université Paris-Diderot, 5 place Jules Janssen, 92195 Meudon, France
e-mail: [nicolas.biver;dominique.bockelee;jacques.crovisier]@obspm.fr

Received 3 March 2012 / Accepted 4 July 2012

ABSTRACT

Context. Submillimeter spectroscopic observations of comets provide an important tool for understanding their chemical composition and enable a taxonomic classification.
Aims. We aim to determine the production rates of several parent- and product volatiles and the $^{12}C/^{13}C$ isotopic carbon ratio in the long-period comet C/2004 Q2 (Machholz), which is likely to originate from the Oort Cloud.
Methods. The line emission from several molecules in the coma was measured with high signal-to-noise ratio in January 2005 at heliocentric distance of 1.2 AU by means of high-resolution spectroscopic observations using the Submillimeter Telescope (SMT) at the Arizona Radio Observatory (ARO).
Results. We have obtained production rates of several volatiles (CH_3OH, HCN, $H^{13}CN$, HNC, H_2CO, CO, and CS) by comparing the observed and simulated line-integrated intensities. We calculated the synthetic profiles using a radiative transfer code that includes collisions between neutrals and electrons, and the effects of radiative pumping of the fundamental vibrational levels by solar infrared radiation. Furthermore, multiline observations of the CH_3OH $J = 7$–6 series allow us to estimate the rotational temperature using the rotation diagram technique. We find that the CH_3OH population distribution of the levels sampled by these lines can be described by a rotational temperature of 40 ± 3 K. Derived mixing ratios relative to hydrogen cyanide are $CO/CH_3OH/H_2CO/CS/HNC/H^{13}CN/HCN = 30.9/24.6/4.8/0.57/0.031/0.013/1$ assuming a pointing offset of 8″ due to the uncertain ephemeris at the time of the observations and the telescope pointing error.
Conclusions. The measured relative molecular abundances in C/2004 Q2 (Machholz) are between low- to typical values of those obtained in Oort Cloud comets, suggesting that it has visited the inner solar system previously and undergone thermal processing. The HNC/HCN abundance ratio of ∼3.1% is comparable to that found in other comets, accounting for the dependence on the heliocentric distance, and could possibly be explained by ion-molecule chemical processes in the low-temperature atmosphere. From a tentative $H^{13}CN$ detection, the measured value of 97 ± 30 for the $H^{12}CN/H^{13}CN$ isotopologue pair is consistent with a telluric value. The outgassing variability observed in the HCN production rates over a period of two hours is consistent with the rotation of the nucleus derived using different observational techniques.

Key words. comets: individual: C/2004 Q2 (Machholz) – molecular processes – radiative transfer – techniques: spectroscopic – submillimeter: planetary systems

1. Introduction

Comets spend most of their lifetime in the outer solar system and therefore have not undergone much thermal processing. Line emission from cometary atmospheres at submillimeter and radio wavelengths is a very useful tool for studying their physical and chemical conditions and relation with other bodies in the solar system (Biver et al. 2002; Bockelée-Morvan et al. 2004). The coma structure and expansion velocity can be derived by fitting the observed line shapes using a molecular excitation code. In addition, mixing ratios of volatiles such as CH_3OH, CO and CS can be compared with observed chemical abundances in protoplanetary disks to improve our understanding of planet formation processes.

The composition of comets has been investigated in the last two decades to develop a classification based on abundances of primary chemical species that displays a great compositional diversity (A'Hearn et al. 1995; Mumma et al. 2003; Bockelée-Morvan et al. 2004). More than 20 parent volatile

* Based on observations carried out with the 10-m Submillimeter Telescope at the Arizona Radio Observatory, Steward Observatory, Mount Graham, Arizona, USA.
† *Current address*: Department of Astrophysical Sciences, Princeton University, NJ 08544, USA.

species that release directly from ices in the nucleus, in addition to several radicals and ions formed by photodissociation in the coma, have been detected via ground-based spectroscopic surveys at infrared and submillimeter wavelengths and in situ measurements. The composition of some cometary ices show strong evidence of processing in the solar nebula and can provide clues about their place of formation and subsequent evolution. The abundance of HCN relative to water has been observed to be roughly constant with a value of 0.1% in several comets for a wide range of heliocentric distances (Biver et al. 2002). Other species show a wide spread of production rates. For instance, CH_3OH has been found to have a variable abundance relative to water, ranging between less than 0.15% to 6% at different heliocentric distances (Bockelée-Morvan et al. 2004). There is no evident correlation between the observed relative abundances and the dynamical class of the comets. Water is the most dominant volatile species and is typically used to determine relative abundances. Although water is not directly accessible from the ground at submillimeter wavelengths, it has been observed from space using the Submillimeter Wave Astronomical Satellite (SWAS), *Odin* and *Herschel* satellites (Neufeld et al. 2000; Lecacheux et al. 2003; Hartogh et al. 2009) or inferred by observations of the hydroxyl (OH) radical at radio wavelengths (Crovisier et al. 2002). *Herschel*'s Heterodyne Instrument for the Far Infrared (HIFI) is able to determine water production rates accurately (Hartogh et al. 2010). Direct measurements of water can also be performed using ground-based telescopes by observations of non-resonance fluorescence emission at infrared wavelengths (Mumma et al. 1986; Bonev et al. 2009).

Comet C/2004 Q2 (Machholz) was discovered on 27 August 2004 by Donald E. Machholz (Machholz et al. 2004). The comet passed perihelion on 24 January 2005 at a heliocentric distance of $r_h = 1.205$ AU and geocentric distance of $\Delta = 0.435$ AU. During its closest approach to Earth at a distance of 0.35 AU on 6 January 2005 it reached a naked-eye visual magnitude of $m_v \sim 3.5$ as reported in the International Comet Quarterly. Owing to its favorable viewing geometry in the northern hemisphere, the comet was extensively observed from the ground at various wavelengths. C/2004 Q2 (Machholz) is a long-period highly eccentric comet whose origin is most likely the Oort Cloud according to the comet classification scheme by Levison (1996), with an approximate initial orbital period of 118 000 years and eccentricity of 0.9994658 before the comet was perturbed gravitationally in the inner solar system (Marsden 2004; Nakano 2006). These values are close to the perihelion osculating elements (see Marsden 2005, JPL Small-Body Database[1]). Its dynamical classification is still a matter of debate because of the strong non-gravitational forces that make a backward orbital integration very unreliable.

In this paper we present high-resolution spectroscopic observations of several volatiles from comet C/2004 Q2 (Machholz) acquired at the Submillimeter Telescope (SMT). Seven species are detected, namely CH_3OH, HCN, HNC, H_2CO, CO, CS, and a marginal detection of $H^{13}CN$. The comet was observed shortly pre-perihelion in January 2005 when it was at a distance ~0.36 AU from Earth. These observations provide information about the outgassing of several molecules and an isotopologue of HCN relative to HCN, which is often used as a proxy for water in cometary taxonomies. We calculate the CH_3OH rotational temperature of the ground vibrational level from several rotational lines and production rates for the observed molecules using a radiative transfer code to fit the observed line intensities. Section 2 presents our SMT observations of comet C/2004 Q2 (Machholz) and the reduction method. In Sect. 3 the radiative transfer models and analysis of the observations are described. Finally, we discuss the obtained results in Sect. 4.

2. Observations

A spectral line survey of primary volatile species in comet C/2004 Q2 (Machholz) was made using the SMT telescope located at the Mount Graham International Observatory (MGIO), a division of Steward Observatory on Mount Graham, Arizona (Baars & Martin 1996; Baars et al. 1999). The SMT has a parabolic 10-m primary dish and a hyperbolic secondary reflector. The observations were performed with the 0.8 mm double-sideband receiver using various spectrometers (Villanueva et al. 2005; de Val-Borro et al. 2011). Detected emission lines may have a different gain response depending upon which sideband the lines were observed in. Thus, the sideband gain ratio (G_{USB}/G_{LSB}) deviates from unity and introduces an additional uncertainty of ~10% in the absolute brightness temperature calibration. A typical system temperature of 150 K was attained during the observations. We observed the comet simultaneously with the chirp transform spectrometer (CTS) with a bandwidth of 215 MHz, and the acousto-optical spectrometers (AOSA, AOSB and AOSC) with total bandwidths of 1 GHz, 970 MHz and 250 MHz, respectively. The spectral resolution provided was 40 kHz for the CTS, and 934, 913 and 250 kHz for the AOSA, AOSB and AOSC. One of the purposes of the observations was to test the performance of the newly installed high-resolution CTS built at the Max Planck Institute for Solar System Research (Hartogh & Hartmann 1990; Villanueva & Hartogh 2004; Villanueva et al. 2006). High spectral resolution is crucial for resolving the shape of rotational lines in comets and study the gas velocity and asymmetries related to non-isotropic outgassing.

Comet C/2004 Q2 (Machholz) was observed near perihelion during six nights in the period 13–18 UT January 2005. Here we focus on the observations acquired on the first four nights with good observing conditions. The data were taken using the standard position switching observing mode, where a reference sky position separated from the comet by 0.°5 was observed for the same amount of time and subtracted from the on-source observations. We used a 30-s exposure for the source and reference positions with 8-min scans. A summary of the observing log with the total integration times for each line is shown in Table 1.

The main beam equivalent brightness temperature scale, T_{mB}, was corrected for the beam efficiency of the telescope estimated from observations of Mars and Saturn in the interval fall 2007–spring 2008[2] and calibrated using the chopper-wheel method (Ulich & Haas 1976). The frequency scale was converted into Doppler velocities in the nucleus frame and corrected for the relative motion of the comet with respect to the observer. We used orbital elements provided by the JPL HORIZONS system[3] to track the comet and the ephemeris to calculate the position and relative motion of the comet with respect to the telescope. Our observing strategy included pointing and calibration observations approximately every hour. The pointing of the telescope was checked and corrected by dedicated reference observations of bright sources like Saturn, the protobinary system W3(OH) and the massive star-forming region DR21(OH)

[1] http://ssd.jpl.nasa.gov/sbdb.cgi?sstr=C/2004+Q2

[2] http://kp12m.as.arizona.edu/smt_docs/smt_beam_eff.htm

[3] http://ssd.jpl.nasa.gov/?horizons

Table 1. Log of the SMT observations of comet C/2004 Q2 (Machholz) in January 2005.

Date[a] (UT)	Molecule	Transition	N^b	Integration[c] (min)	$\langle r_h \rangle^d$ (AU)	$\langle \Delta \rangle^e$ (AU)	$\langle \phi \rangle^f$	Beam size
12.96	HCN	4–3	13	107.2	1.220	0.361	42.°5	20.″93
	H_2CO	4–3						21.″09
13.20	CO	3–2	33	270.6	1.219	0.362	42.°6	21.″46
	CS	7–6						21.″64
	$H^{13}CN$	4–3						21.″49
	CH_3OH	13_1–13_0A^-						21.″65
13.95	CH_3OH	7–6	16	133.0	1.217	0.365	43.°3	21.″93
14.17	HNC	4–3	22	183.0	1.217	0.366	43.°5	20.″46
15.14	HNC	4–3	39	329.2	1.215	0.371	44.°2	20.″46
16.16	CO	3–2	47	378.0	1.213	0.376	45.°0	21.″46
	CS	7–6						21.″64
	$H^{13}CN$	4–3						21.″49
	CH_3OH	13_1–13_0A^-						21.″65

Notes. In some receiver tunings several lines were observed simultaneously in the lower and upper sidebands. [(a)] Start times in universal time (UT) fractional day values. [(b)] Number of individual scans. [(c)] Total integration time. [(d)] Heliocentric distance. [(e)] Geocentric distance. [(e)] Solar phase angle (Sun-C/2004 Q2 (Machholz)-Earth).

because they were close to the comet. Typical pointing errors were ∼4″, i.e., about a quarter of the half-power beam width (HPBW) at the observed frequencies.

These observations were very challenging owing to the relatively uncertain ephemeris of C/2004 Q2 (Machholz) since they were carried out about five months after the comet was discovered, and particularly because of the strong non-gravitational forces needed to reproduce the observations afterwards. Its orbit changed significantly during its passage through the inner solar system due to planetary perturbations from an initial orbital parameter of $a_0^{-1} = 0.000404$ AU^{-1} to a future value of 0.001856 AU^{-1} (Marsden 2004). At the time of the observations, the comet was moving with a fast apparent motion of ∼300″ per hour in the sky relative to the background stars. This introduced an additional term of uncertainty in the pointing accuracy. Comparing the ephemeris actually used for the tracking with the HORIZONS ephemeris calculated from the after-the-fact orbit including non-gravitational accelerations, we obtain an average pointing offset of 4″. Including the effect of the telescope pointing error, the offset was at maximum 8″. This value was considered in our computation of the production rates for the observed species shown in Table 2.

The data analysis was performed using the CLASS analysis software, which is part of GILDAS package[4], in conjunction with the NumPy and SciPy libraries of high-level mathematical tools (Jones et al. 2001; Oliphant 2007). A standing wave appears as a baseline ripple in some of the spectra. We determined the baseline by fitting a polynomial to the emission-free background and subtracted it from the original spectrum. After removal of the standing wave, the individual scans were averaged to increase the signal-to-noise ratio (S/N). Line intensities were calculated from the weighted averages of the spectra where the statistical weights are the inverse square of the root mean square (rms) noise of each individual spectrum.

The comet's heliocentric distance was in the range r_h = 1.213–1.220 AU, and the geocentric distance was Δ = 0.361–0.376 AU during the observing period (see Table 1). The HPBW of the telescope varied between 20.″5 and 22″ at different frequencies, corresponding to 6600 and 6900 km projected on the comet, so that molecules from the outer coma contribute to the detected emission. The line excitation in this region is dominated by collisions between neutrals and electrons, and infrared fluorescence by solar radiation. During the observing run the solar phase angle (Sun-C/2004 Q2 (Machholz)-Earth) ranged from 42.°5 to 45.°0. We detected seven species (CH_3OH, HCN, $H^{13}CN$, HNC, H_2CO, CO, and CS), whose spectra are shown in Figs. 1, 2 and 4–9. The observations were focused on the study of the hydrogen cyanide chemistry with the detection of HCN, HNC and a tentative detection of $H^{13}CN$ to determine the isotopic $^{12}C/^{13}C$ ratio, as well as other volatile species that sublimate directly from the nucleus into the coma and abundant daughter species.

In Table 2 we show a comparison of the mixing ratios of the detected species with respect to H_2O with those derived from infrared observations on similar dates (Bonev et al. 2009; Kobayashi & Kawakita 2009). For species that are detected in several nights during our observing run, the mixing ratios refer to the weighted average of the observed spectra. Table 3 shows the molecules and transitions detected in our survey with 1-σ uncertainties. Line frequencies were obtained from the latest online edition of the JPL Molecular Spectroscopy Catalog (Pickett et al. 1998). Most transitions were observed with the higher resolution CTS, which resolves the line shape, and the AOS backends simultaneously. Integrated line intensities shown in Table 3 were obtained integrating over velocities in the interval [–2, 2] km s^{-1} unless another line overlaps within that region. Doppler shifts in the comet rest frame were obtained as the first moment of the velocity over the same interval ($\sum_i T_{\mathrm{mB}i} v_i / \sum_i T_{\mathrm{mB}i}$ where v is the Doppler velocity and the index i refers to the channel number).

3. Results

3.1. Radiative transfer modeling

We adopted a molecular excitation and radiative transfer model based on the Sobolev escape probability method, which includes collisional effects and infrared fluorescence by solar radiation to derive the production rates (Bockelée-Morvan 1987; Biver 1997; Biver et al. 1999). In the outer coma, solar infrared pumping of vibrational bands followed by instantaneous spontaneous decay establishes a fluorescence equilibrium. To test the effect of the infrared excitation, an independent molecular excitation model

[4] http://www.iram.fr/IRAMFR/GILDAS

Table 2. Comparison of production rates of detected species relative to HCN and H_2O in comet C/2004 Q2 (Machholz) with statistical uncertainties.

Molecule	Q^a (molec. s^{-1})	Q/Q_{HCN}	$Q/Q_{H_2O}{}^b$ (%)	$Q/Q_{H_2O}{}^c$ (%)	$Q/Q_{H_2O}{}^d$ (%)
HCN	$(2.26 \pm 0.02) \times 10^{26}$	1	0.084 ± 0.001	$0.15^{+0.01}_{-0.02}$	0.16 ± 0.01
CO	$(7.0 \pm 0.6) \times 10^{27}$	30.9 ± 2.6	2.6 ± 0.2	5.07 ± 0.51	
CH_3OH	$(5.5 \pm 0.6) \times 10^{27}$	24.6 ± 2.5	2.1 ± 0.2	2.14 ± 0.12 1.54 ± 0.07^e	1.2 ± 0.1 1.65 ± 0.09^e
H_2CO	$(3.87 \pm 0.20) \times 10^{26}$	1.7 ± 0.1	0.14 ± 0.01	0.11 ± 0.03	0.18 ± 0.01
	$(1.09 \pm 0.06) \times 10^{27}{}^f$	4.8 ± 0.3	0.41 ± 0.02		
CS	$(1.15 \pm 0.04) \times 10^{26}$	$(5.1 \pm 1.7) \times 10^{-1}$	$(4.3 \pm 0.1) \times 10^{-2}$		
	$(1.29 \pm 0.04) \times 10^{26}{}^f$	$(5.7 \pm 1.9) \times 10^{-1}$	$(4.8 \pm 0.2) \times 10^{-2}$		
HNC	$(7 \pm 2) \times 10^{24}$	$(3.1 \pm 0.9) \times 10^{-2}$	$(2.6 \pm 0.7) \times 10^{-3}$		
$H^{13}CN$	$(3 \pm 1) \times 10^{24}$	$(1.3 \pm 0.5) \times 10^{-2}$	$(1.1 \pm 0.4) \times 10^{-3}$		

Notes. [a] Weighted mean of production rates measured at the SMT on 13–16 January 2005 derived from excitation and radiative transfer models assuming a pointing offset of 8″. [b] A water production rate of $Q_{H_2O} = 2.7 \times 10^{29}$ molec. s^{-1} was used to derive the mixing ratios, intermediate between the measurement on 20 January 2005 by the *Odin* satellite (Biver et al. 2007b) and the value derived from observations at infrared wavelengths on 19 January 2005 (Bonev et al. 2009). [c] Weighted mean of mixing ratios obtained on 28–29 November 2004 and 19 January 2005 with NIRSPEC on the Keck II 10-m telescope (Bonev et al. 2009). [d] Mixing ratios obtained on 30 January 2005 with NIRSPEC on the Keck II 10-m telescope (Kobayashi & Kawakita 2009). [e] Revised CH_3OH mixing ratios from Villanueva et al. (2012). [f] Production rates for H_2CO and CS assume the presence of an extended source described in the text.

based on the publicly available accelerated Monte Carlo radiative transfer code *ratran* was used to calculate the populations of the rotational levels as a function of the distance from the nucleus for various molecules and line emission in the cometary coma (Hogerheijde & van der Tak 2000)[5]. This code includes collisional effects with water molecules and electrons, but neglects the pumping by solar infrared radiation from the ground-state vibrational level. We used the one-dimensional spherically symmetric version of the code following the description outlined in Bensch & Bergin (2004), which has been extensively tested and used to interpret *Herschel* cometary observations (see e.g. Hartogh et al. 2010; de Val-Borro et al. 2010; Hartogh et al. 2011).

The radial gas density profiles for parent molecules H_2O, CH_3OH, HCN, $H^{13}CN$, HNC, and CO were obtained using the standard Haser spherically symmetric distribution for parent volatiles (Haser 1957):

$$n_p(r) = \frac{Q}{4\pi r^2 v_{exp}} \exp\left(-\frac{r\beta_p}{v_{exp}}\right), \quad (1)$$

where Q is the total production rate in molecules s^{-1}. The photodissociation rate β_p takes into account the dissociation and ionization of molecules by the solar UV radiation, v_{exp} is the expansion velocity and r is the nucleocentric distance. However, second-generation molecules such as HNC, CS and H_2CO are not correctly described by this profile. In the last two cases, the density profile of daughter species originating from the photodissociation of an extended parent source in the coma is given by (Combi et al. 2004)

$$n_d(r) = \frac{Q}{4\pi r^2 v_{exp}} \frac{\beta_p}{\beta_d - \beta_p} \left(\exp\left(-\frac{r\beta_p}{v_{exp}}\right) - \exp\left(-\frac{r\beta_d}{v_{exp}}\right)\right), \quad (2)$$

where β_p and β_d are the parent and daughter photodissociation rates. We obtained the photodissociative lifetimes for CH_3OH, HCN, HNC, H_2CO and CO from Crovisier (1994) assuming the quiet-Sun reference spectrum, and the CS radical lifetime was taken from Biver et al. (2011). The photodissociation rates were scaled by the heliocentric distance of C/2004 Q2 (Machholz) at the time of the observations. Deviations from a spherically symmetric Haser distribution due to anisotropic outgassing were not considered.

Neutrals in cometary atmospheres are excited by collisions with other molecules and electrons, which are the dominant effects in the inner coma, and radiative pumping of the fundamental vibrational levels by the solar infrared flux. Infrared pumping of vibrational bands by solar radiation contributes to the excitation in the outer coma where the gas and electron densities are low (Bockelée-Morvan 1987). Most of the detected emission in comet C/2004 Q2 (Machholz) originates from a region in which molecules are in an excitation state intermediate between fluorescence and collision-dominated equilibrium.

Collision rates with water and electrons were obtained for several molecules from the current version of the Leiden Atomic and Molecular Database[6] (LAMDA; Schöier et al. 2005). When collision rates with water were not available, we scaled the collision rates with molecular hydrogen by the ratio of their molecular weights. However, the calculated line intensities of the rotational transitions in the ground-based vibrational level are weakly dependent on the collision cross-sections – of about a few percent.

We used a water production rate of $Q_{H_2O} = 2.7 \times 10^{29}$ molec. s^{-1}, close to the *Odin* satellite measurement on 20 January 2005 of $(2.64 \pm 0.08) \times 10^{29}$ molec. s^{-1} derived from the observation of the fundamental transition at 557 GHz (Biver et al. 2007b) at $r_h = 1.208$ AU, and to the water production rates of $(2.73 \pm 0.07) \times 10^{29}$ molec. s^{-1} and $(2.76 \pm 0.08) \times 10^{29}$ molec. s^{-1} derived from observations at infrared wavelengths on 19 January 2005 (Bonev et al. 2006, 2007, 2009). Excitation parameters in the model are the neutral gas kinetic temperature, which controls the molecular excitation in the collisional region, and the electron density. We assumed a gas kinetic temperature of 60 K and the rotational temperature derived from the relative line intensities of the $J = 7$–6 transitions for CH_3OH. The electron density and temperature profiles from Biver (1997)

[5] The source code is available from *ratran*'s website at http://www.sron.rug.nl/~vdtak/ratran/frames.html

[6] http://www.strw.leidenuniv.nl/~moldata/

Table 3. Rotational emission lines in comet C/2004 Q2 (Machholz) observed by SMT on 13–16 January 2005.

Molecule	Label[a]	Date[b] (UT)	Transition	Frequency[c] (GHz)	$\int T_{mB}\,dv$ (K km s^{-1})	Velocity shift[d] (m s^{-1})	Q^e (molec. s^{-1})	Q^f (molec. s^{-1})	Uncertainty[g] (molec. s^{-1})
HCN[h]		12.96	4–3	354.505476	3.962 ± 0.033	−31 ± 7	(1.87 ± 0.02) × 10^{26}	(2.26 ± 0.02) × 10^{26}	0.34 × 10^{26}
H_2CO[i]		12.96	5_{15}–4_{14}	351.768645	0.675 ± 0.035	−783 ± 65	(9.64 ± 0.50) × 10^{26}	(1.09 ± 0.06) × 10^{27}	1.64 × 10^{26}
CO		13.20	3–2	345.795989	0.194 ± 0.012	200 ± 38	(5.66 ± 0.35) × 10^{27}	(6.81 ± 0.42) × 10^{27}	1.02 × 10^{27}
CS[i]		13.20	7–6	342.882850	0.550 ± 0.010	−50 ± 29	(1.15 ± 0.02) × 10^{26}	(1.37 ± 0.03) × 10^{26}	0.17 × 10^{26}
CH_3OH		13.20	13_1–13_0A^-	342.729796	0.212 ± 0.010	−826 ± 28	(5.84 ± 0.28) × 10^{27}	(7.07 ± 0.33) × 10^{27}	1.1 × 10^{27}
CH_3OH	(1)		7_0–6_0E	338.124488	0.468 ± 0.021	−358 ± 97			
CH_3OH	(2)		7_{-1}–$6_{-1}E$	338.344588	0.644 ± 0.021	−101 ± 21			
CH_3OH	(3)		7_0–6_0A^+	338.408698	0.633 ± 0.021	−41 ± 93			
CH_3OH	(4)		7_{-4}–$6_{-4}E$	338.504065	0.048 ± 0.021	−58 ± 93			
CH_3OH			7_4–6_4A^+	338.512632					
CH_3OH	(5)		7_4–6_4A^-	338.512644	0.313 ± 0.021	−114 ± 55			
CH_3OH			7_2–6_2A^-	338.512853					
CH_3OH	(6)		7_4–6_4E	338.530257	0.037 ± 0.021	−162 ± 132			
CH_3OH	(7)	13.95	7_3–6_3A^+	338.540826	0.296 ± 0.027	−48 ± 98	(4.55 ± 0.47) × 10^{27}	(5.48 ± 0.56) × 10^{27}	0.82 × 10^{27}
CH_3OH	(8)		7_3–6_3A^-	338.543152					
CH_3OH	(9)		7_{-3}–$6_{-3}E$	338.559963	0.146 ± 0.021	−61 ± 335			
CH_3OH	(10)		7_3–6_3E	338.583216	0.150 ± 0.021	−300 ± 144			
CH_3OH	(11)		7_1–6_1E	338.614936	0.466 ± 0.023	−353 ± 40			
CH_3OH	(12)		7_2–6_2A^+	338.639802	0.349 ± 0.024	−212 ± 70			
CH_3OH	(13)		7_2–6_2E	338.721693	0.744 ± 0.031	−389 ± 55			
CH_3OH			7_{-2}–$6_{-2}E$	338.722898					
CH_3OH	(14)		7_1–6_1A^-	341.415615	0.613 ± 0.021	−374 ± 29			
HNC[h]		14.17	4–3	362.630303	0.100 ± 0.039	457 ± 303	(4.2 ± 1.6) × 10^{24}	(5.2 ± 1.8) × 10^{24}	0.7 × 10^{24}
$H^{13}CN$[h,j]		14.94	4–3	345.339759	0.050 ± 0.018		(2.5 ± 0.9) × 10^{24}	(3 ± 1) × 10^{24}	0.5 × 10^{24}
HNC[h]		15.14	4–3	362.630303	0.170 ± 0.039	20 ± 137	(7.1 ± 1.6) × 10^{24}	(8.8 ± 2.0) × 10^{24}	1.3 × 10^{24}
CO		16.16	3–2	345.795989	0.205 ± 0.022	119 ± 64	(5.98 ± 0.64) × 10^{27}	(7.20 ± 0.77) × 10^{27}	1.08 × 10^{27}
CS[i]		16.16	7–6	342.882850	0.492 ± 0.024	−50 ± 29	(1.03 ± 0.05) × 10^{26}	(1.22 ± 0.06) × 10^{26}	0.18 × 10^{26}
CH_3OH		16.16	13_1–13_0A^-	342.729796	0.155 ± 0.026	−90 ± 93	(4.27 ± 0.72) × 10^{27}	(5.17 ± 0.87) × 10^{27}	0.78 × 10^{27}

Notes. Observed flux densities integrated over velocity, Doppler velocity shifts and production rates derived using the comet model described in Sect. 3.1 are shown with statistical uncertainties. [a] Labels in Fig. 1. [b] Mid-time of the observations recorded as fractional days in UT. [c] The line frequencies were obtained from the latest online edition of the JPL Molecular Spectroscopy Catalog (Pickett et al. 1998). [d] The velocity offsets are computed with respect to the optocenters of the complete components for blended lines. [e] Production rates assuming a pointing offset of 2″. [f] Production rates assuming a pointing offset of 8″. [g] The uncertainty in the production rates are 1-σ uncertainties considering the receiver sideband gain ratio, main beam efficiency and kinetic temperature errors. [h] Line intensities are the sum of the hyperfine components. [i] Production rates were derived assuming a daughter product extended source distribution with a scale length of L_p = 8000 km for H_2CO and L_p = 650 km for CS. [j] Weighted average of observations obtained on 13.20 and 16.16 UT January.

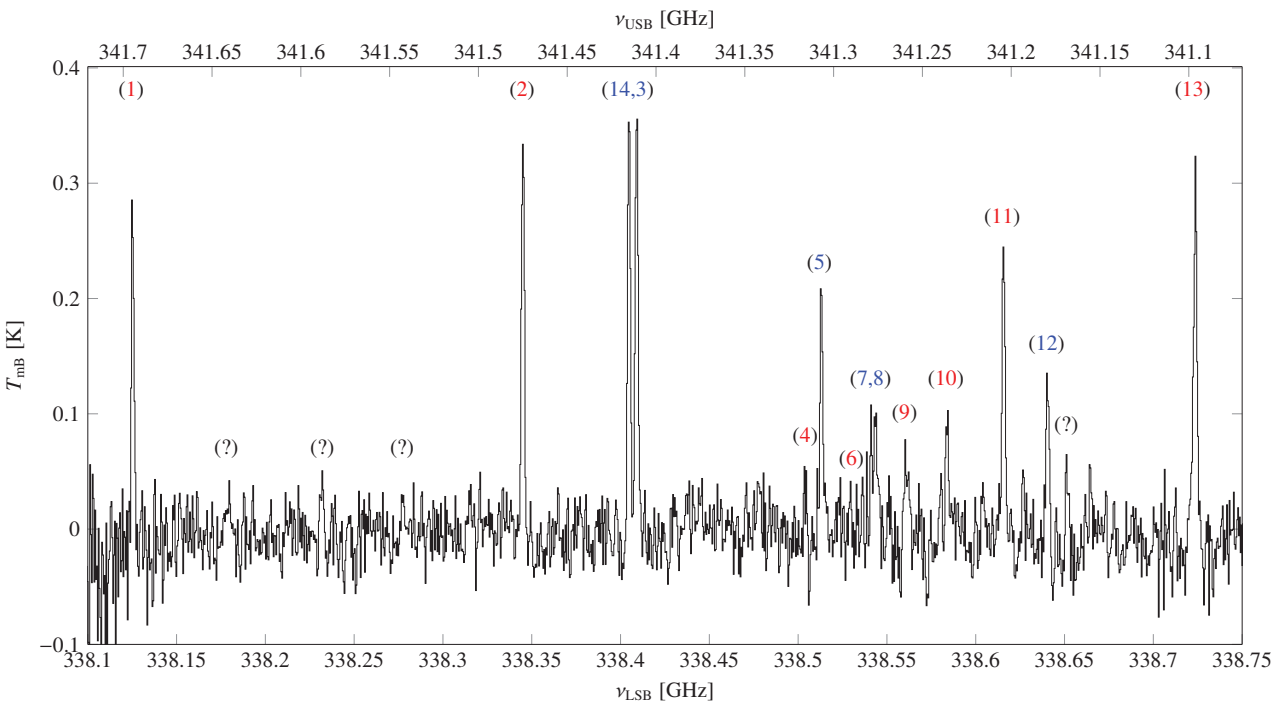

Fig. 1. CH_3OH averaged spectrum obtained on 13.95 UT January 2005. The lower and upper x-axis scales represent the frequency of the lower and upper sidebands, respectively. Labels indicate detected CH_3OH spectral lines listed in Table 3. There is a blend of three A^+ and A^- emission lines at 338.513 GHz (label 5). The observed line at 338.722 GHz is a blend of two E components (label 13). The A^- line at 341.416 GHz (label 14) is in the upper sideband close to the A^+ transition at 338.409 GHz (label 3). A marginal detection of the E line at 338.530 GHz is indicated by label 6. The unidentified emission features labeled by (?) are discussed in Sect. 3.2.

were assumed. Since the electron density in the coma is not a fully known quantity, an electron density scaling factor of $x_{n_e} = 0.5$ with respect to the reference profile deduced from in situ measurements of comet 1P/Halley was used. The expansion velocity is assumed to be constant in the coma, with a value of 0.75 km s^{-1}, obtained from the width of the HCN line. This value is consistent with the shape of several lines observed with the Institut de Radioastronomie Millimétrique (IRAM) 30-m radio telescope at about the same time (Biver et al., in prep.).

The radiative transfer equation was solved by integrating along various lines of sight through the coma that covered 2.5 × HPBW at a given offset from the nucleus, to obtain the brightness distribution in the plane of the sky once the level populations were calculated. The beam-averaged emission was then calculated at the distance of the comet.

Production rates were calculated comparing observed line-integrated intensities with the integrated synthetic lines obtained with the Sobolev escape probability and *ratran* codes by fitting the production rate to the observed line intensity to derive the relative molecular abundances in the nucleus (Bensch & Bergin 2004). Opacity effects are negligible for all lines, therefore the difference in the derived production rates in our models arise only from including the pumping of excited vibrational bands by infrared solar radiation as an excitation mechanism (Bockelée-Morvan & Crovisier 1989). Table 2 summarizes the mixing ratios relative to water and hydrogen cyanide in comet C/2004 Q2 (Machholz). We show the derived production rates with statistical uncertainties for the observed molecules using parent- and daughter density distributions in Table 3. Production rates are affected by pointing errors of up to 8″ since the ephemeris used at the time of the observations was relatively uncertain. Therefore we considered this pointing offset to compute the production rates.

3.2. CH_3OH

Methanol has been observed in several comets with a wide range of abundances since its initial discovery in comet C/1989 X1 (Austin) by Bockelée-Morvan et al. (1990). Methanol rotational lines often appear in multiplets at millimeter and sub-millimeter wavelengths, allowing the estimation of the temperature and excitation conditions in the coma. Rotational states are ordered in non-degenerate A levels and degenerate E levels corresponding to different symmetry states. Radiative transitions between A and E species are strictly forbidden, and collision-induced transitions are highly improbable. We detected twelve A^+, A^- and E-methanol emission lines of the $J = 7$–6 series in C/2004 Q2 (Machholz) at frequencies listed in Table 3. In addition, there is a blend of three emission lines at 338.513 GHz and a blend of two lines at 338.722 GHz. Figure 1 shows the observed CH_3OH rotational spectrum between 338.10 and 338.75 GHz with labels indicating the transitions listed in Table 3. Several unidentified emission features are found at about 338.178, 338.232, 338.277, and 338.651 GHz in the lower sideband and 341.169, 341.543, 341.588, and 341.642 GHz in the upper sideband, which are labeled by (?) in Fig. 1. The line widths of these features are comparable with the detected CH_3OH lines and thus are consistent with a cometary origin, although no plausible lines were found at those frequencies nor the corresponding image band frequencies in the JPL Molecular Spectroscopy Catalog (Pickett et al. 1998) and the Cologne Database for Molecular Spectroscopy (Müller et al. 2001, 2005). Integrated intensities and velocity

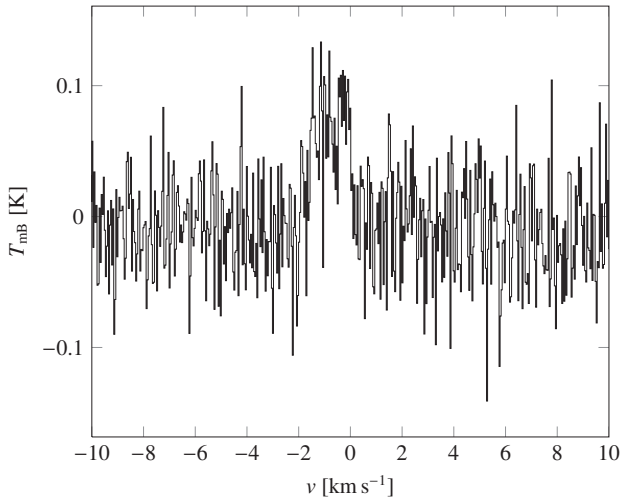

Fig. 2. Averaged spectrum of the CH_3OH (13_1–13_0A^-) line at 342.730 GHz observed on 13.20 and 16.16 UT January with the CTS. The vertical axis is the calibrated main beam brightness temperature and the horizontal axis is the Doppler velocity in the comet rest frame.

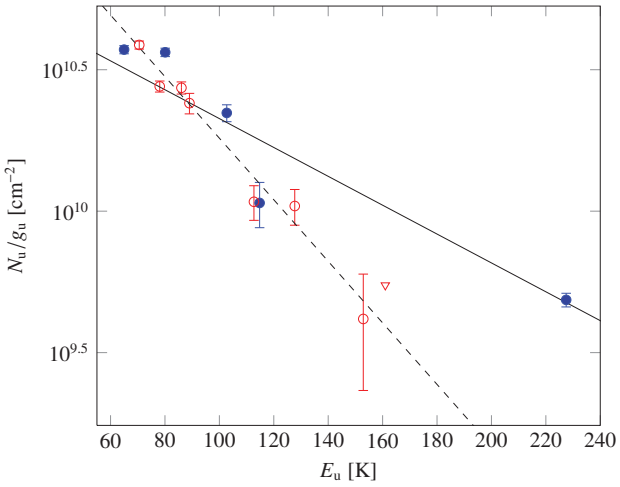

Fig. 3. Rotation diagram for CH_3OH lines in comet C/2004 Q2 (Machholz) including 1-σ uncertainties. The column density of the upper level divided by its degeneracy in logarithmic scale is plotted against the energy of the upper level. Filled (blue) circles are A^+ and A^--CH_3OH lines, empty (red) circles denote E-CH_3OH transitions and the empty (red) triangle indicates the 3-σ upper limit on the $J = 7_4$–6_4E transition at 338.530 GHz. The solid line shows the best linear fit with a derived rotational temperature of 85 ± 7 K. The dashed line shows the best linear fit excluding the $J = 13_1$–13_0A^- transition at 342.730 GHz (energy of the upper state of ∼228 K relative to the ground state) with a derived rotational temperature of 40 ± 3 K.

shifts of the identified CH_3OH lines with statistical uncertainties are shown in Table 3. The observed velocity shifts toward the blue wing suggest asymmetric outgassing with preferential emission in the direction toward the observer, which should be studied with a non-spherically symmetric model. Additionally, we detected serendipitiously a high-excitation-level methanol transition $J = 13_1$–13_0A^- at 342.730 GHz in the CS/CO spectra from 13 and 16 January. Figure 2 shows the averaged CTS spectrum from both dates.

3.2.1. Rotational temperature

The rotational temperature was calculated from the relative intensities of the individual CH_3OH lines between levels with quantum numbers $J = 7$–6 and 13_1–13_0A^- using the rotation diagram technique, assuming that the population distribution of the levels sampled by the emission lines is in local thermodynamical equilibrium (LTE), i.e., described by a Maxwell-Boltzmann distribution characterized by a single temperature. Then the column density of the upper level within the beam, N_u, can be expressed as

$$N_u = N\frac{g_u}{Z(T_{rot})}\exp\left(-\frac{E_u}{k_B T_{rot}}\right), \quad (3)$$

where g_u is the degeneracy of the upper level, Z denotes the partition function, which is a function of temperature, T_{rot} is the rotational temperature, E_u is the energy of upper state, k_B represents the Boltzmann constant, and N is the total column density averaged over the beam. This method is commonly used in studies of the interstellar medium.

A linear fit of $\ln(N_u/g_u)$ versus E_u provides the rotational temperature as the inverse of the slope and the averaged total column density divided by the partition function from its intercept at $E_u = 0$. We included in the analysis the blended transitions at 338.722 and 338.723 GHz starting from the 7_2 and 7_{-2} E levels, and the 338.541 and 338.543 GHz pair from the 7_3 A^+ and 7_3 A^- levels, by assigning half of the observed intensity to a virtual level of intermediate energy (see Bockelée-Morvan et al. 1994b). The high-excitation-level line at 342.730 GHz was included in the rotational diagram analysis. For optically thin conditions, which normally apply to cometary lines of most volatile species, the observed intensity, $\int T_{mB}\,dv$, is proportional to the column density of the upper transition level (Bockelée-Morvan et al. 1994a):

$$N_u = \frac{8\pi k_B \nu_{ul}^2}{hc^3 A_{ul}}\int T_{mB}\,dv, \quad (4)$$

where A_{ul} is the Einstein coefficient for spontaneous emission and v_{ul} the transition frequency.

The rotation diagram for multiple CH_3OH lines that fits both A and E-CH_3OH simultaneously was determined using a weighted linear least-squares method where the weights are equal to the reciprocal of the variance of each line intensity measurement. The standard deviation of the fitted parameters is obtained from the diagonal elements of the covariance matrix. Figure 3 shows the best fit for all observed lines and only the $J = 7$–6 series with statistical uncertainties. In contrast to water, no reliable A/E ratio was retrieved from radio lines for CH_3OH (Pardanaud et al. 2007). This ratio is almost insensitive to temperature, i.e., it significantly departs from the statistical ratio only for very low spin temperatures, because of the small energy difference of the A and E levels. Retrievals of the A/E ratio in CH_3OH for comet C/2001 A2 LINEAR at infrared wavelengths are consistent with $T_{spin} > 18$ K (Villanueva et al. 2012).

The measured rotational temperature in C/2004 Q2 (Machholz) is 85 ± 7 K with 1-σ uncertainty from the linear best fit of the rotational diagram that includes all the observed methanol lines on 13.20, 13.95 and 16.16 UT January (solid line in Fig. 3). The high-excitation line $J = 13_1$–13_0A^- is too bright, indicating that the LTE assumption is not valid for that transition. Weighted least-squares fitting methods are known to be very sensitive to points that are substantially farther away from the linear relation than expected. For a non-thermal population

distribution, a different rotational temperature is anticipated for the $J = 13_1$–13_0A^- line and thus the LTE model is not applicable to all the data. In addition, the observations were not simultaneous and variability in the outgassing rate is likely to be present. If the $J = 13_1$–13_0A^- line is excluded from the rotation diagram analysis, a rotational temperature of 40 ± 3 K is derived (dashed line in Fig. 3).

Rotational temperatures of 76 ± 2 K in HCN and 93 ± 2 K in H_2O were obtained on 19 January 2005 with the Near InfraRed echelle SPECtrograph (NIRSPEC) instrument at the Keck II telescope (Bonev et al. 2009). Kawakita & Kobayashi (2009) found a rotational temperature of 85 ± 5 K in H_2O and 90^{+10}_{-8} K in CH_4 on 30 January 2005. Retrievals of the ortho-to-para ratios in H_2O in C/2004 Q2 (Machholz) at infrared wavelengths are consistent at 95% confidence level with $T_{spin} > 34$ K (Bonev et al. 2007) and $T_{spin} > 27$ K (Kawakita & Kobayashi 2009). From the A/E/F relative abundances in CH_4 the lower limits are $T_{spin} > 35$–38 K (Bonev et al. 2009) and $T_{spin} > 27$ K (Kawakita & Kobayashi 2009). The nuclear spin temperature is defined as the rotational temperature retrieved from a given spin isomers abundance ratio assuming their respective population distributions are in LTE conditions. These observations at infrared wavelengths prove the collision-dominated inner region of the coma where the population levels are roughly in thermal equilibrium, and the rotational temperature is expected to be similar to the kinetic temperature only in the collisional region (Bockelée-Morvan et al. 1994a). However, the derived rotational temperature of CH_3OH at 338 GHz is likely to be different from the kinetic temperature because of relaxation of the population levels toward fluorescence equilibrium. We could not determine the rotational temperature for other gas species because no other simultaneous line observations were obtained. Therefore a kinetic temperature of 60 K was assumed in the excitation modeling for other species.

3.2.2. Production rate from the rotational diagram

We derived a CH_3OH beam-averaged column density of $\langle N\rangle/Z(T_{rot}) = (2.22 \pm 0.45) \times 10^{11}$ cm^{-2} from the intercept of the linear fit of the $J = 7$–6 transitions in the rotational diagram at $E_u = 0$. Assuming that the population of methanol levels is close to a Boltzmann distribution, the derived column density is a good approximation of the real distribution in the coma. Accordingly, we omitted the transition $J = 13_1$–13_0A^- in deriving the column density for the reasons outlined in Sect. 3.2.1. We computed the partition function evaluated at the rotation temperature by performing a logarithmic interpolation between the values from Villanueva et al. (2012). These partition functions were computed using two million CH_3OH levels for the range $T = 1$–500 K. The resulting column density is $\langle N\rangle = (8.8 \pm 3.2) \times 10^{13}$ cm^{-2} including the 1-σ uncertainty in the partition function introduced by T_{rot}. A methanol production rate of $Q_{CH_3OH} = (6.8 \pm 2.5) \times 10^{27}$ molec. s^{-1} was derived from the column density assuming a Haser parent molecule distribution with a constant expansion velocity of 0.75 km s^{-1} and a beam-pointing offset of 8″ from the nucleus, corresponding to a mixing ratio relative to water of ~2.5%. On the other hand, from the excitation model described in Sect. 3.1, a production rate of $Q_{CH_3OH} = (5.5 \pm 0.6) \times 10^{27}$ molec. s^{-1} was estimated from the $J = 7$–6 transitions assuming that $T_{kin} = T_{rot}$ and the same pointing offset, which corresponds to a relative abundance relative to water of ~2.1%. This mixing ratio represents an intermediate value in comparison with other Oort Cloud comets.

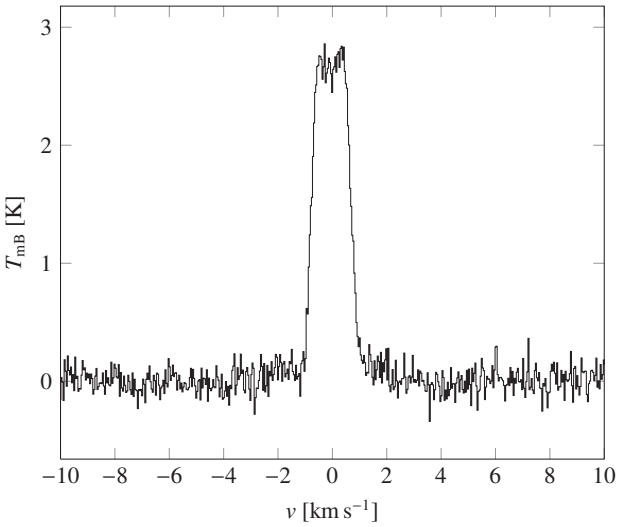

Fig. 4. HCN (4–3) multiplet at 354.505 GHz observed with the CTS on 12.96 UT January with a 6420 s total on-source integration time. The vertical axis is the main beam brightness temperature scaled by the beam efficiency of SMT and the horizontal axis is the Doppler velocity in the rest frame of the nucleus.

3.3. HCN

The HCN transitions are the brightest emission lines in cometary atmospheres for ground-based submillimeter observations (Schloerb et al. 1987; Bockelée-Morvan et al. 1994b; Drahus et al. 2010). Its production rate has been found to be in a roughly constant ratio with respect to water, therefore it is often used to derive relative molecular abundances. Figure 4 shows the HCN $J = 4$–3 rotational line at 354.505 GHz observed by the CTS. The line is detected with a very high S/N of ~100 after about two hours of integration. The intensity and velocity shift of the observed HCN emission line intensity are shown in Table 3. From the width of the line we obtain an estimate of 0.75 km s^{-1} for the coma expansion velocity. Expansion velocities in the range $v_{exp} = 0.5$–0.8 km s^{-1} are typical for comets at this heliocentric distance and for this gas production rate (Tseng et al. 2007). Because HCN has a short rotational lifetime, it is important to model its excitation including collisional and radiative processes, which control the population levels in the outer coma. We derive an HCN production rate of $(2.26 \pm 0.02) \times 10^{26}$ molec. s^{-1} assuming the kinetic temperature to be equal to 60 K. The water production rate was assumed to be $Q_{H_2O} \sim 2.5 \times 10^{29}$ molec. s^{-1}, which corresponds to an HCN/H_2O mixing ratio of about 0.08%. This value is moderately lower than the standard ratio of 0.1% observed at radio wavelengths for several comets over a wide range of heliocentric distances (Biver et al. 2002; Bockelée-Morvan et al. 2004).

3.4. $H^{13}CN$

Owing to the strong activity of C/2004 Q2 (Machholz) and its close approach to Earth during our observational campaign, it was possible to search for weak transitions of rare isotopic species. The $H^{13}CN$ $J = 4$–3 transition at 345.340 GHz was observed simultaneously with the CS and CO transitions on 14.20 and 16.16 UT January with a total integration time of ~640 min, and is marginally detected by averaging the observations from both days (see Fig. 5). The inferred production

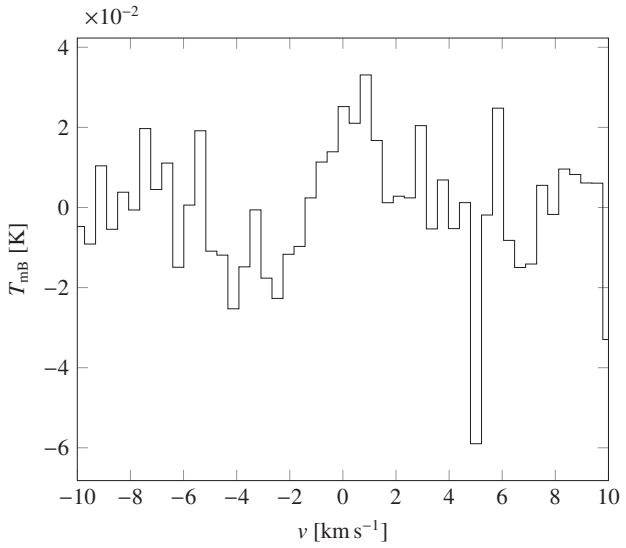

Fig. 5. Averaged spectrum of the $H^{13}CN$ (4–3) multiplet at 345.340 GHz observed on 13.20 and 16.16 UT January with the low-resolution AOS. The vertical axis is the calibrated main beam brightness temperature and the horizontal axis is the Doppler velocity in the comet rest frame. This line is outside the CTS and AOSC frequency ranges.

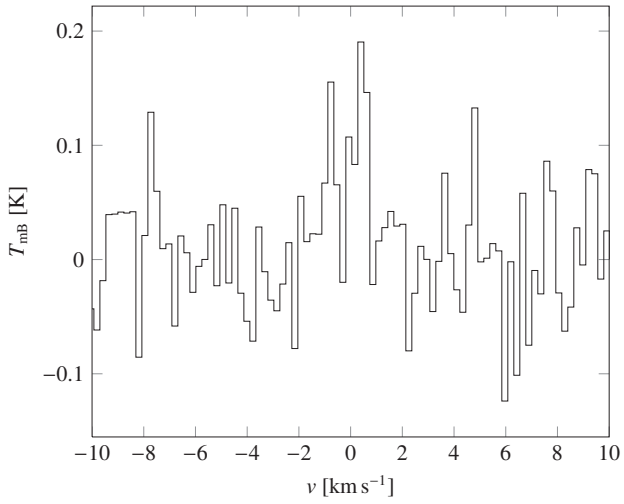

Fig. 6. Averaged spectrum of the HNC (4–3) multiplet at 362.630 GHz observed on 14.17 and 15.14 UT January with the CTS. The vertical axis is the main beam brightness temperature and the horizontal axis is the Doppler velocity in the comet rest frame. The effective resolution after smoothing is 200 m s^{-1}.

rate is $(3 \pm 1) \times 10^{24}$ molec. s^{-1}. The derived $^{12}C/^{13}C$ isotopic ratio of 97 ± 30 is consistent with the standard solar value of 89 observed in various comets. Isotopic fractionation is very sensitive to chemical and physical conditions where the molecules condensed and therefore provide important clues about how cometary material formed in the early solar system. If comets originate from different regions in the solar nebula, they could display variation in their isotopic composition depending on the local temperature. Additional measurements of the $^{12}C/^{13}C$ ratio in HCN have been obtained in comets C/1995 O1 (Hale-Bopp) (Jewitt et al. 1997; Ziurys et al. 1999) and 17P/Holmes (Bockelée-Morvan et al. 2008), which are consistent with a solar value. The carbon isotopic composition of several comets of different dynamical families also agrees with a solar value from measurements of C_2 and CH (see Jehin et al. 2009; Bockelée-Morvan 2011, for reviews on the isotopic composition of cometary volatiles).

3.5. HNC

Hydrogen isocyanide (HNC) is a metastable isomer of HCN and has been detected in several comets with a measured HNC/HCN ratio ranging between 0.03–0.3 (Lis et al. 2008). Figure 6 shows the HNC spectrum in C/2004 Q2 (Machholz) observed by the CTS. A production rate of $(7 \pm 2) \times 10^{24}$ molec. s^{-1} is derived, corresponding to a relative abundance of 3.1% relative to HCN, a typical abundance for moderately active comets. The origin of cometary HNC is still a debated topic. HNC is an abundant species that may be produced by chemical reactions from parent volatile species in the coma. Models have shown that HNC could also be formed in the coma via ion-neutral and isomerization chemical reactions (Irvine et al. 1998). Consequently, determining the production rate is important to distinguish between single parent volatile and multiple precursors for HNC. Since we do not have precise estimates on its distribution, we assumed the Haser formula for a parent molecule in our computation of the production rate.

3.6. H_2CO

Formaldehyde is a common molecule in the interstellar medium and has been detected in more than 20 comets at radio wavelengths since the first unequivocal detection at millimeter wavelengths of the 3_{12}–2_{11} line at 226 GHz in comet C/1989 X1 (Austin) (Colom et al. 1992). Solid-phase hydrogenation reactions on the surface of the nucleus could account for the presence of formaldehyde and have been confirmed recently by laboratory experiments (Nagaoka et al. 2005; Hidaka et al. 2009). Figure 7 shows the H_2CO 5_{15}–4_{14} transition at 351.769 GHz in comet C/2004 Q2 (Machholz) obtained by the AOS. CTS and high-resolution AOS data are not available for this transition. It is possible that the frequency scale in this range of the AOS can be slightly inaccurate. For the acousto-optical backends, the correspondence between channel number and frequency is not quite linear, and the correction may be important and ill-known on the border of the band. This line is detected in the lower sideband of the AOS at about 300 MHz from the central frequency with a total bandwidth of ∼1 GHz. The same H_2CO line was observed at the Caltech Submillimeter Observatory (CSO) on similar dates (12.1 and 13.1 January) where the velocity shift toward the blue wing was found to be about twice smaller (Biver et al., in prep.).

H_2CO has ortho- and para spin isomers that differ in the alignment of the nuclear spin of the H atoms (parallel in the ortho state and anti-parallel in the para state). We assumed that cometary formaldehyde has an ortho-to-para ratio of 3 according to the nuclear spin statistical weights ratio. H_2CO is a short-lived molecule and its spatial distribution has been found to differ from that expected for a parent molecule. An extended source of H_2CO has been identified in several comets (Meier et al. 1993; Bockelée-Morvan et al. 1994b). Assuming that H_2CO originates either from the nucleus or from an extended source with a parent scale length of $L_p = 8000$ km, production rates vary between $(3.87 \pm 0.20) \times 10^{26}$ molec. s^{-1} and $(1.09 \pm 0.06) \times 10^{27}$ molec. s^{-1}, respectively, as inferred by a model with an 8″ average pointing offset (Biver 1997). The first value represents a lower limit because it is expected that direct release from the nucleus underestimates the real H_2CO production rate. The corresponding

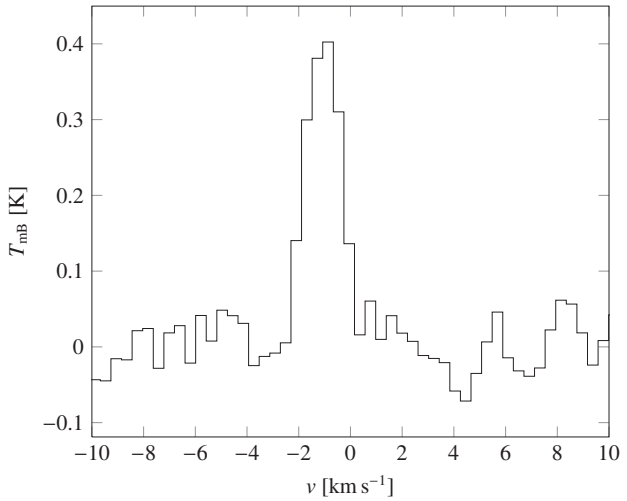

Fig. 7. H_2CO (5_{15}–4_{14}) transition at 351.769 GHz observed on 12.96 UT January with the lower resolution AOS. The vertical axis is the main beam brightness temperature and the horizontal axis is the Doppler velocity in the comet rest frame. This line is outside the CTS and AOSC frequency ranges. The frequency scale in the range close to the border of the AOS can be slightly inaccurate.

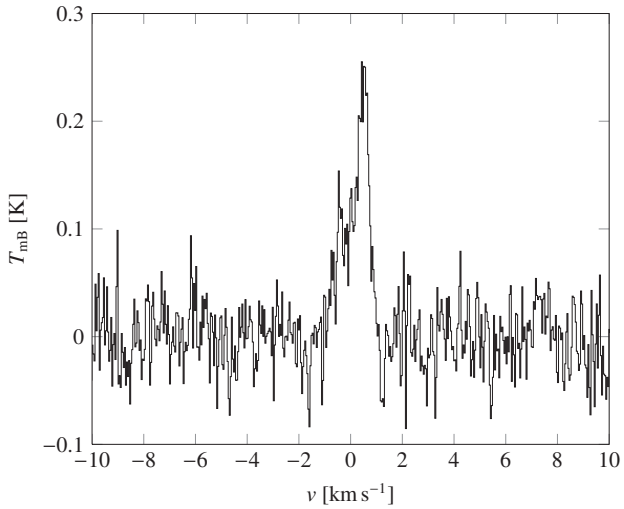

Fig. 8. CO (3–2) transition at 345.796 GHz observed on 14.94 UT January with the CTS. The asymmetric line profile suggests a strong anisotropic outgassing with preferential production in the direction opposite to the Sun.

Q_{H_2CO}/Q_{H_2O} mixing ratios are 0.14% and 0.41% for the parent source and extended H_2CO source production. These values are intermediate in comparison with the observed mixing ratios in other Oort Cloud comets (Bockelée-Morvan 2011).

3.7. CO

We show the carbon monoxide $J = 3$–2 line in Fig. 8. The line profile is strongly asymmetric with a peak in the redshifted wing. There is some observational evidence that the CO lines may be affected by self-absorption effects in CO-rich and very active comets, which have been included in our analysis (Bockelée-Morvan et al. 2010). For the observed CO transition in comet C/2004 Q2 (Machholz) our model predicts an optical depth of $\tau \sim 0.2$. Therefore, the observed excess emission at redshifted frequencies is attributable to kinematic effects by the presence of a jet roughly in the antisolar direction since the solar phase angle was small during the observations. An anisotropic outgassing radiative transfer model with a rotating jet-like structure would provide a better fit to the line shape (see e.g. Bockelée-Morvan et al. 2009). Based on an isotropic coma distribution and using a kinetic gas temperature of 60 K, we deduce a CO production rate of $(7.0 \pm 0.6) \times 10^{27}$ molec. s^{-1}. CO is thought to be a parent molecule with a small additional contribution from dissociation of CO_2 and we used the Haser parent molecule distribution to derive the CO production for simplicity.

Oort Cloud comets are expected to be enriched in hypervolatile species such as CO and the abundance ratio of H_2CO and CO has been observed to be correlated in several comets. We find a relative abundance of CO with respect to HCN of about 31 and a mixing ratio of ~2.6% relative to H_2O in C/2004 Q2 (Machholz). Observations of the hypervolatile CO in comets at infrared and radio frequencies show a wide range of abundances (Bockelée-Morvan et al. 2004). CO abundances observed at radio wavelengths range between ~0.4–20% relative to H_2O (Bockelée-Morvan 2011). Generally, these lines are relatively weak because of the small CO dipole, although they are the most readily observed cometary lines at large heliocentric distances. The CO abundance in eight Oort Cloud comets observed by infrared ground-based spectroscopy ranged between ~1–20% relative to water (Mumma et al. 2003). Thus the measured Q_{CO}/Q_{H_2O} mixing ratio lies toward the low end of the observed range in Oort Cloud comets. Depletion of CO would therefore suggest that C/2004 Q2 (Machholz) has been injected into the inner solar system before and is not a dynamically new comet.

3.8. CS

The CS radical is believed to be produced in cometary coma from carbon disulfide (CS_2) and has been observed in several comets in the UV and radio wavelengths (Feldman et al. 2004; Bockelée-Morvan et al. 2004). Figure 9 shows the observed CS $J = 7$–6 emission line at 342.883 GHz. The line profile is asymmetric with a peak in the redshifted side that resembles the CO $J = 3$–2 line shape shown in Fig. 8. This suggests an anisotropic outgassing in the anti-sunward direction. It is expected that the line is optically thin and absorption effects in the foreground are negligible according to our model. To obtain the density profile we used a photodissociation rate of $\beta_{CS} = 2.5 \times 10^{-5}$ molec. s^{-1} at $r_h = 1$ AU derived from spectroscopic observations (Boissier et al. 2007; Biver et al. 2011). This photodissociation rate corresponds to a scale-length of 28 000 km, assuming an expansion velocity of 0.75 km s^{-1} obtained from the width of the HCN line. A CS production rate of $(1.15 \pm 0.04) \times 10^{26}$ molec. s^{-1} is estimated from a spherically symmetric model with direct release from the nucleus. Assuming a distributed source in the coma with scale length $L_p = 650$ km, which corresponds to production from CS_2 (Boissier et al. 2007), a production rate of $(1.29 \pm 0.04) \times 10^{26}$ molec. s^{-1} is inferred. The derived mixing ratio with respect to water of ~0.04% is lower than the typical value measured in other comets at radio wavelengths (Bockelée-Morvan 2011; Crovisier et al. 2009a).

3.9. Short-term outgassing variability

Several comets have shown periodic variations in the outgassing that are associated with the rotation of the nucleus, combined

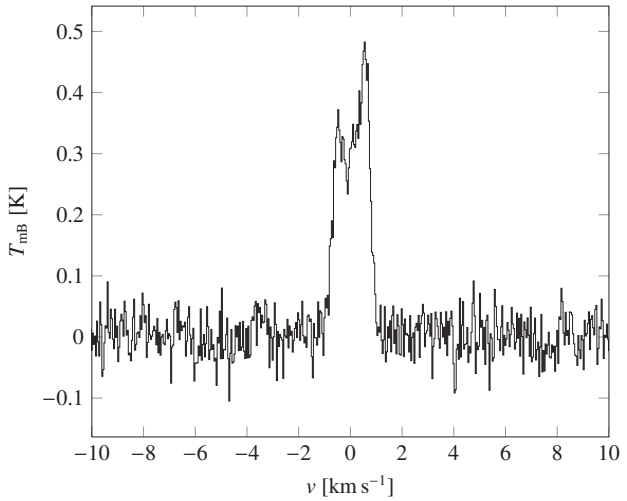

Fig. 9. CS (7–6) emission line at 342.883 GHz observed on 14.94 UT January with the CTS. A double-peaked profile is observed. The velocity scale in the horizontal axis is in the comet rest frame.

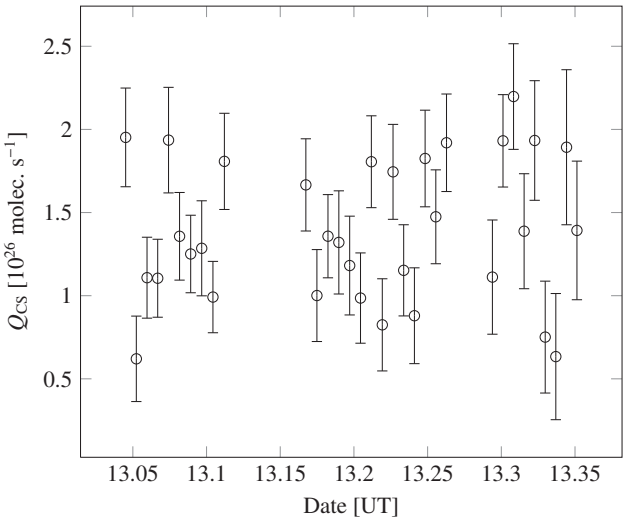

Fig. 11. Time evolution of the retrieved CS production rates in comet C/2004 Q2 (Machholz) on 13 January 2005. Each data point represents an 8-min observation with statistical uncertainties.

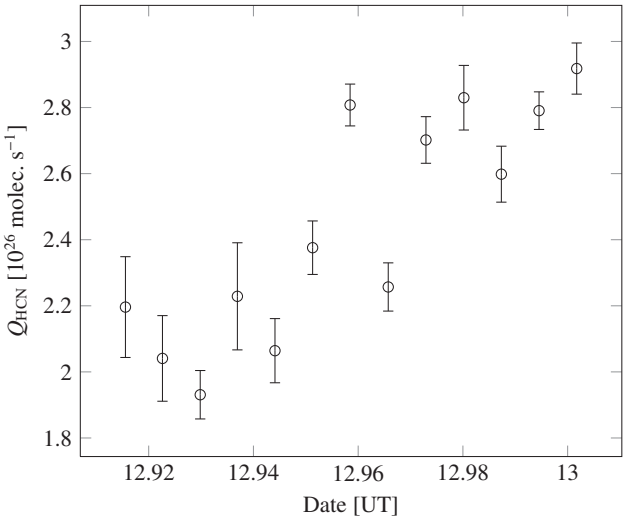

Fig. 10. HCN production rates in comet C/2004 Q2 (Machholz) as a function of time on 12–13 January 2005. Each data point represents an 8-min observation.

with a long-term seasonal variation with a peak emission close to perihelion. In some cases, the rotation periods of cometary nuclei have been determined by measuring this periodic outgassing variability using various techniques (see Samarasinha et al. 2004, for a review). Rotation periods have been derived from the periodic variability of the HCN production rate in comets 9P/Tempel 1 (Biver et al. 2007a), 73P-C/Schwassmann-Wachmann 3 (Drahus et al. 2010) and 2P/Encke (Jockers et al. 2011). To address the question of short-term periodic variability in the production rates of C/2004 Q2 (Machholz), we selected the HCN and CS observations from one night, 12–13 January, which have sufficient S/N.

The production rates for each individual scan of the HCN observations are shown in Fig. 10. The HCN $J = 4$–3 line was detected in each single 8-min scan with an S/N of ∼15. We observe an increase of the production rate by roughly 40% during the 2-h observing interval with a mean value of $(2.09 \pm 0.02) \times 10^{26}$ molec. s^{-1}, although the first scans at the beginning of the observations were obtained at lower elevation starting at 45° and could be affected by stability problems in the instrument or changes in the main beam efficiency. The HCN evolution suggests a periodic variation in the activity of the comet potentially induced by the rotation of the nucleus due to the presence of active regions on the surface. The large amplitude of the variation can be explained by an intrinsic activity change as one or more active areas are exposed to solar radiation during the rotation cycle. This variation is compatible with the rotation periods of 9.1 ± 0.2 h derived by Reyniers et al. (2009) from broadband filter optical photometry, 9.1 ± 1.9 h reported by Sastri et al. (2005) from studying dust fans visible in R-band images, 17.60 ± 0.05 h from narrowband CN images reported by Farnham et al. (2007), and 17.8 ± 0.5 h by determining the inner coma morphology from photometric variations (Manzini et al. 2012). However, we are not able to perform a detailed periodicity analysis of the HCN production curve due to the insufficient temporal coverage because the total time span of our observations is less than one night. Hence it is not possible to determine if the brightness increase is a periodic phenomenon or due to non-periodic activity changes.

Figure 11 shows the evolution of the CS outgassing rate on 13 January during a period of 7.5 h. The CS line is relatively strong and has one of the highest peak antenna temperatures after the HCN line. CS is detected in most of the individual 8-min scans with an S/N between 3–6. The comet displayed a strong variability with a 40% variation around the mean value. It is likely that this brightness variability is not a periodic event. Small outbursts or activity changes are expected as comets approach the Sun, which could explain the observed variability (A'Hearn et al. 2005). It is also possible that the strong fluctuations in the CS production could be partly explained by pointing uncertainties that affect the derived production rates combined with instrument instabilities. Observations of the CS line on 16 January have a lower S/N and only in a fraction of the individual scans the line is detected with at least a 3-σ confidence level.

4. Discussion

We have observed several molecular species in comet C/2004 Q2 (Machholz) when it was close to perihelion in the sub-millimeter wavelength range with the SMT during six consecutive nights in January 2005. These observations led to the detection of several CH_3OH, HCN, $H^{13}CN$, HNC, H_2CO, CO, and CS rotational lines. Our main goal was to measure the relative production rates of several parent and daughter volatiles in this comet and estimate the CH_3OH rotational temperature. We derive an HCN production rate of $(2.26 \pm 0.03) \times 10^{26}$ molec. s^{-1} at heliocentric distance of 1.2 AU, which corresponds to a $Q_{HCN}/Q_{H_2O} \sim 0.08\%$, using a spherically symmetric radiative transfer numerical code that includes collisional effects between neutrals and electrons and radiative pumping of the fundamental vibrational levels by solar radiation (Bockelée-Morvan & Crovisier 1989). In addition to the statistical noise, the precision of the production rates is affected by the limited pointing accuracy at the time the observations were performed. An 8″ pointing offset was included in the computation of the production rates, which results in ∼20% uncertainty in the derived values. Mixing ratios relative to hydrogen cyanide and water are listed in Table 2 for the production rates derived from the weighted average value of the observations on different dates during our campaign. The asymmetric shape of the CO and CS line profiles suggests that there is preferential outgassing from the anti-sunward side of the nucleus, while the HCN and H_2CO line profiles are fairly symmetric, although the latter is shifted toward the blue wing perhaps due to an instrumental effect. Using the rotational diagram technique, we retrieve a cold rotational temperature of 40 ± 3 K for the methanol energy levels sampled by the J = 7–6 transitions.

Retrieved molecular abundances relative to water are comparable to those obtained in Oort Cloud comets (Biver et al. 2002; Crovisier et al. 2009b; Dello Russo et al. 2011). Our Q_{HCN}/Q_{H_2O} mixing ratio of ∼0.084% is slightly lower than the typical value of 0.1% observed at radio wavelengths, and 50% lower than those found by Bonev et al. (2009) from averaged 28 November 2004 and 19 January 2005 observations and by (Kobayashi & Kawakita 2009) from observations on 30 January 2005 using the same instrument. The observed difference between our measurement of the HCN mixing ratio and those derived at infrared wavelengths is fairly typical. The mixing ratio of CH_3OH relative to H_2O agrees with the infrared measurement in comet C/2004 Q2 (Machholz) by Bonev et al. (2009) performed on 19 January 2005 at r_h = 1.208 AU that is closer in time with our observations. Considering the pointing uncertainty that introduces an error of ∼20%, our measurement is consistent within 1-σ with the revised abundances retrieved from the infrared observations on 19 and 30 January 2005 by Villanueva et al. (2012) using a new line-by-line model for the ν_3 fundamental band of CH_3OH. The averaged CO production rate measured on 13 and 16 January agrees with that obtained by Bonev et al. (2009) on 29 November 2004 at r_h = 1.493 AU ($(6.3 \pm 0.3) \times 10^{27}$ molec. s^{-1}) within confidence limits. In contrast, the Q_{CO}/Q_{H_2O} mixing ratio of ∼2.6% is almost a factor of two lower than that derived by Bonev et al. (2009). For a parent molecule distribution, the derived Q_{H_2CO}/Q_{H_2O} ratio is 0.14%, and Q_{H_2CO}/Q_{HCN} is 1.7%, which is more reliable since these molecules were observed simultaneously. These values are intermediate between those measured by Bonev et al. (2009) and (Kobayashi & Kawakita 2009). On the other hand, the values inferred from a daughter molecule extended source distribution with a scale length of L_p = 8000 km are about a factor of 3 higher. This illustrates that the derived production rates depend strongly on the assumed scale length of the parent molecule. This is particularly the case for H_2CO where the beam size is slightly smaller than L_p, so it may be possible that this value overestimates the production rate. An HNC abundance of 3.1% with respect to HCN is found assuming direct release from the nucleus with a Haser distribution (3.0% if infrared pumping of the fundamental vibrational levels is not considered), which suggests that this molecule may be destroyed by chemical reactions. This value is compatible with those observed in other comets given the dependence on heliocentric distance – except 73P/Schwassmann-Wachmann and the very active Hale-Bopp (C/1995 O1) (see Lis et al. 2008).

Outgassing variations induced by the nucleus rotation are expected to appear from non-sphericity of the nucleus or the presence of active region areas on the surface. The variability observed in the HCN and CS outgassing rates on 12–13 January is affected by inaccurate pointing, which introduces an uncertainty of about the expected variation caused by the rotation of the nucleus. HCN production rates show a uniform brightness increase over a period of two hours, which could be a periodic phenomenon consistent with the rotation period of the nucleus derived using different methods (Sastri et al. 2005; Farnham et al. 2007; Reyniers et al. 2009; Manzini et al. 2012), but our observations do not provide sufficient phase coverage to constrain the rotation period.

Comets are the most pristine objects in the solar system and have not undergone substantial thermal processing. Cometary ices are more sensitive to thermal processing than dust. Hence their abundances provide indications about the formation and evolution of material in the early solar nebula. Dynamically new comets are expected to be enriched in volatile species, and CO is the most volatile component observed in C/2004 Q2 (Machholz). However, our observations show a relative depletion of CO and and an intermediate-range mixing ratio of H_2CO and CH_3OH compared to the range of values measured in other comets (Biver et al. 2002). It is believed that the composition of icy material on the surface of the nucleus is altered by the exposure to solar radiation. Thus, these observations provide a hint about its thermal/dynamical history and suggest that the comet has visited the inner solar system previously. Formation regions of comets of Oort Cloud comets vary from 5–30 AU from the protosun according to the standard "Nice model" scenario (Morbidelli et al. 2008) and can be constrained by observations of the chemical composition. The relative depletion of several volatiles in C/2004 Q2 (Machholz) agrees with the determination of the formation region in the inner region of the solar nebula compared with other Oort Cloud comets, derived from the lower limit of the retrieved nuclear spin temperatures and dynamical models of the evolution of planetesimals in the solar system (Kobayashi & Kawakita 2009; Kawakita & Kobayashi 2009).

Submillimeter spectroscopy of cometary atmospheres is a useful approach for studying the diversity of species that sublimate when a comet approaches the Sun. These observations demonstrate the capabilities of the new CTS based on digital technology installed at the SMT to support solar system observation programs, further established with the cometary observations presented in Küppers et al. (2004); Villanueva & Hartogh (2004); Drahus et al. (2010); Paganini et al. (2010); Jockers et al. (2011), and observations of the Venusian mesosphere in Rengel et al. (2008a,b). Our observations of comet C/2004 Q2 (Machholz) were analyzed for noise properties, standing wave and spectral line properties as compared to model predictions. The spectrometer is found to perform according to its

original specification in terms of sensitivity, spectral resolution and stability.

Acknowledgements. The SMT is operated by the Arizona Radio Observatory (ARO), Steward Observatory, University of Arizona. We are grateful to the ARO staff for their support during these observations. This work was supported by the Special Priority Program 1488 of the German Science Foundation. M.dV.B. acknowledges fruitful discussions with Michal Drahus during the course of this work. We thank the referee, Michael F. A'Hearn, for helpful comments that improved the manuscript.

References

A'Hearn, M. F., Millis, R. L., Schleicher, D. G., Osip, D. J., & Birch, P. V. 1995, Icarus, 118, 223
A'Hearn, M. F., Belton, M. J. S., Delamere, W. A., et al. 2005, Science, 310, 258
Baars, J. W. M., & Martin, R. N. 1996, in Rev. Mod. Astron., 9, ed. R. E. Schielicke, 111
Baars, J. W. M., Martin, R. N., Mangum, J. G., McMullin, J. P., & Peters, W. L. 1999, PASP, 111, 627
Bensch, F., & Bergin, E. A. 2004, ApJ, 615, 531
Biver, N. 1997, Ph.D. Thesis, Univ. Paris 7-Diderot
Biver, N., Bockelée-Morvan, D., Crovisier, J., et al. 1999, AJ, 118, 1850
Biver, N., Bockelée-Morvan, D., Crovisier, J., et al. 2002, Earth Moon and Planets, 90, 323
Biver, N., Bockelée-Morvan, D., Boissier, J., et al. 2007a, Icarus, 187, 253
Biver, N., Bockelée-Morvan, D., Crovisier, J., et al. 2007b, Planet. Space Sci., 55, 1058
Biver, N., Bockelée-Morvan, D., Colom, P., et al. 2011, A&A, 528, A142
Bockelée-Morvan, D. 1987, A&A, 181, 169
Bockelée-Morvan, D. 2011, in IAU Symp., 280, 261
Bockelée-Morvan, D., & Crovisier, J. 1989, A&A, 216, 278
Bockelée-Morvan, D., Crovisier, J., Colom, P., Despois, D., & Paubert, G. 1990, in ESA Spec. Publ., 315, ed. B. Battrick, 143
Bockelée-Morvan, D., Crovisier, J., Colom, P., & Despois, D. 1994a, A&A, 287, 647
Bockelée-Morvan, D., Padman, R., Davies, J. K., & Crosivier, J. 1994b, Planet. Space Sci., 42, 655
Bockelée-Morvan, D., Crovisier, J., Mumma, M. J., & Weaver, H. A. 2004, in Comets II, eds. M. C. Festou, H. U. Keller, & H. A. Weaver (Univ. Arizona Press), 391
Bockelée-Morvan, D., Biver, N., Jehin, E., et al. 2008, ApJ, 679, L49
Bockelée-Morvan, D., Henry, F., Biver, N., et al. 2009, A&A, 505, 825
Bockelée-Morvan, D., Boissier, J., Biver, N., & Crovisier, J. 2010, Icarus, 210, 898
Boissier, J., Bockelée-Morvan, D., Biver, N., et al. 2007, A&A, 475, 1131
Bonev, B. P., Mumma, M. J., DiSanti, M. A., et al. 2006, ApJ, 653, 774
Bonev, B. P., Mumma, M. J., Villanueva, G. L., et al. 2007, ApJ, 661, L97
Bonev, B. P., Mumma, M. J., Gibb, E. L., et al. 2009, ApJ, 699, 1563
Colom, P., Crovisier, J., Bockelee-Morvan, D., Despois, D., & Paubert, G. 1992, A&A, 264, 270
Combi, M. R., Harris, W. M., & Smyth, W. H. 2004, Gas dynamics and kinetics in the cometary coma: theory and observations, eds. M. C. Festou, H. U. Keller, & H. A. Weaver (Univ. Arizona Press), 523
Crovisier, J. 1994, J. Geophys. Res., 99, 3777
Crovisier, J., Colom, P., Gérard, E., Bockelée-Morvan, D., & Bourgois, G. 2002, A&A, 393, 1053
Crovisier, J., Biver, N., Bockelée-Morvan, D., et al. 2009a, Earth Moon and Planets, 105, 267
Crovisier, J., Biver, N., Bockelée-Morvan, D., & Colom, P. 2009b, Planet. Space Sci., 57, 1162
de Val-Borro, M., Hartogh, P., Crovisier, J., et al. 2010, A&A, 521, L50
de Val-Borro, M., Jarchow, C., Hartogh, P., Villanueva, G., & Küppers, M. 2011, Adv. Geosci., 25, 149
Dello Russo, N., Vervack, Jr., R. J., Lisse, C. M., et al. 2011, ApJ, 734, L8
Drahus, M., Küppers, M., Jarchow, C., et al. 2010, A&A, 510, A55
Farnham, T. L., Samarasinha, N. H., Mueller, B. E. A., & Knight, M. M. 2007, AJ, 133, 2001
Feldman, P. D., Cochran, A. L., & Combi, M. R. 2004, Spectroscopic investigations of fragment species in the coma, eds. M. C. Festou, H. U. Keller, & H. A. Weaver (Univ. Arizona Press), 425
Hartogh, P., & Hartmann, G. K. 1990, Measurement Science and Technology, 1, 592
Hartogh, P., Lellouch, E., Crovisier, J., et al. 2009, Planet. Space Sci., 57, 1596
Hartogh, P., Crovisier, J., de Val-Borro, M., et al. 2010, A&A, 518, L150
Hartogh, P., Lis, D. C., Bockelée-Morvan, D., et al. 2011, Nature, 478, 218
Haser, L. 1957, Bull. Soc. Roy. Sci. Liege, 43, 740
Hidaka, H., Watanabe, M., Kouchi, A., & Watanabe, N. 2009, ApJ, 702, 291
Hogerheijde, M. R., & van der Tak, F. F. S. 2000, A&A, 362, 697
Irvine, W. M., Bergin, E. A., Dickens, J. E., et al. 1998, Nature, 393, 547
Jehin, E., Manfroid, J., Hutsemékers, D., Arpigny, C., & Zucconi, J.-M. 2009, Earth Moon and Planets, 105, 167
Jewitt, D., Matthews, H. E., Owen, T., & Meier, R. 1997, Science, 278, 90
Jockers, K., Szutowicz, S., Villanueva, G., Bonev, T., & Hartogh, P. 2011, Icarus, 215, 153
Jones, E., Oliphant, T., Peterson, P., et al. 2001, SciPy: Open source scientific tools for Python, http://www.scipy.org/
Kawakita, H., & Kobayashi, H. 2009, ApJ, 693, 388
Kobayashi, H., & Kawakita, H. 2009, ApJ, 703, 121
Küppers, M., Hartogh, P., & Villanueva, G. 2004, in AAS/Division for Planetary Sciences Meeting Abstracts, BAAS, 36, 1125
Lecacheux, A., Biver, N., Crovisier, J., et al. 2003, A&A, 402, L55
Levison, H. F. 1996, in Completing the Inventory of the Solar System, eds. T. Rettig, & J. M. Hahn, ASP Conf. Ser., 107, 173
Lis, D. C., Bockelée-Morvan, D., Boissier, J., et al. 2008, ApJ, 675, 931
Machholz, D. E., Garradd, G., & McNaught, R. H. 2004, IAU Circ., 8394
Manzini, F., Behrend, R., Comolli, L., et al. 2012, Ap&SS, 337, 531
Marsden, B. G. 2004, Minor Planet Electronic Circulars, 2004-U31
Marsden, B. G. 2005, Minor Planet Circulars, 54558, 1
Meier, R., Eberhardt, P., Krankowsky, D., & Hodges, R. R. 1993, A&A, 277, 677
Morbidelli, A., Levison, H. F., & Gomes, R. 2008, The Dynamical Structure of the Kuiper Belt and Its Primordial Origin, eds. M. A. Barucci, H. Boehnhardt, D. P. Cruikshank, A. Morbidelli, & R. Dotson, 275
Müller, H. S. P., Thorwirth, S., Roth, D. A., & Winnewisser, G. 2001, A&A, 370, L49
Müller, H. S. P., Schlöder, F., Stutzki, J., & Winnewisser, G. 2005, J. Mol. Struct., 742, 215
Mumma, M. J., Weaver, H. A., Larson, H. P., Williams, M., & Davis, D. S. 1986, Science, 232, 1523
Mumma, M. J., Disanti, M. A., dello Russo, N., et al. 2003, Adv. Space Res., 31, 2563
Nagaoka, A., Watanabe, N., & Kouchi, A. 2005, ApJ, 624, L29
Nakano, S. 2006, Oriental Astronomical Association, Nakano Notes Circular, NK 1352, http://www.oaa.gr.jp/~oaacs/nk/nk1352.htm
Neufeld, D. A., Stauffer, J. R., Bergin, E. A., et al. 2000, ApJ, 539, L151
Oliphant, T. E. 2007, Comput. Sci. Engin., 9, 10
Paganini, L., Villanueva, G. L., Lara, L. M., et al. 2010, ApJ, 715, 1258
Pardanaud, C., Crovisier, J., Bockelée-Morvan, D., & Biver, N. 2007, in SF2A-2007: Proceedings of the Annual meeting of the French Society of Astronomy and Astrophysics, eds. J. Bouvier, A. Chalabaev, & C. Charbonnel, 421
Pickett, H. M., Poynter, R. L., Cohen, E. A., et al. 1998, J. Quant. Spec. Radiat. Transf., 60, 883
Rengel, M., Hartogh, P., & Jarchow, C. 2008a, Planet. Space Sci., 56, 1688
Rengel, M., Hartogh, P., & Jarchow, C. 2008b, Planet. Space Sci., 56, 1368
Reyniers, M., Degroote, P., Bodewits, D., Cuypers, J., & Waelkens, C. 2009, A&A, 494, 379
Samarasinha, N. H., Mueller, B. E. A., Belton, M. J. S., & Jorda, L. 2004, Rotation of cometary nuclei, eds. M. C. Festou, H. U. Keller, & H. A. Weaver (Univ. Arizona Press), 281
Sastri, J. H., Vasundhara, R., Kuppuswamy, K., & Velu, C. 2005, IAU Circ., 8480, 3
Schloerb, F. P., Kinzel, W. M., Swade, D. A., & Irvine, W. M. 1987, A&A, 187, 475
Schöier, F. L., van der Tak, F. F. S., van Dishoeck, E. F., & Black, J. H. 2005, A&A, 432, 369
Tseng, W.-L., Bockelée-Morvan, D., Crovisier, J., Colom, P., & Ip, W.-H. 2007, A&A, 467, 729
Ulich, B. L., & Haas, R. W. 1976, ApJS, 30, 247
Villanueva, G., & Hartogh, P. 2004, Exper. Astron., 18, 77
Villanueva, G. L., Küppers, M., & Hartogh, P. 2005, in BAAS, 37, 633
Villanueva, G. L., Hartogh, P., & Reindl, L. M. 2006, IEEE Transactions on Microwave Theory Techniques, 54, 1415
Villanueva, G. L., DiSanti, M. A., Mumma, M. J., & Xu, L.-H. 2012, ApJ, 747, 37
Ziurys, L. M., Savage, C., Brewster, M. A., et al. 1999, ApJ, 527, L67